PAPER

Check for updates

First-principles calculations on monolayer WX$_2$ (X = S, Se) as an effective drug delivery carrier for anti-tuberculosis drugs†

Khaled Mahmud,‡ Taki Yashir‡ and Ahmed Zubair [ID] *

Tuberculosis (TB) remains a major global health concern, necessitating the exploration of novel drug delivery systems to combat the challenges posed by conventional approaches. We investigated the potential of monolayer transition metal dichalcogenides (TMDs) as an innovative platform for efficient and targeted delivery of antituberculosis drugs. Specifically, the electronic and optical properties of prominent TB drugs, isoniazid (INH) and pyrazinamide (PZA), adsorbed on tungsten diselenide (WSe$_2$) and tungsten disulfide (WS$_2$) monolayers were studied using first-principles calculations based on density functional theory (DFT). The investigation revealed that the band gaps of WSe$_2$ and WS$_2$ monolayers remain unaltered upon adsorption of PZA or INH, with negative adsorption energy indicating stable physisorption. We explored different vertical and horizontal configurations, and the horizontal ones were more stable. When INH and PZA drugs were horizontally adsorbed together on WSe$_2$, the most stable configuration was found with an adsorption energy of −2.35 eV. Moreover, the adsorbed drugs could be readily released by light within the visible or near-infrared (NIR) wavelength range. This opened up possibilities for their potential application in photothermal therapy, harnessing the unique properties of these 2D materials. The comprehensive analysis of the band structures and density of states provides valuable insights into how the drug molecules contributed to the conduction and valence bands. The optical responses of anti-TB drugs adsorbed in 2D WSe$_2$ and WS$_2$ were similar to those of pristine 2D WSe$_2$ and WS$_2$. We demonstrated the temperature-dependent release mechanism of our 2D WSe$_2$ and WS$_2$ drug complexes, confirming the feasibility of releasing the discussed anti-tuberculosis drugs by generating heat through photothermal therapy. These findings hold significant promise for developing innovative drug delivery systems that have enhanced efficacy for targeted and low-toxic TB treatment.

1 Introduction

TB is an infectious fatal disease and is one of the deadliest diseases worldwide. A bacterium called *Mycobacterium tuberculosis* primarily attacks the lungs and causes this infection.[1] Despite antibiotics being developed, an estimated 10.6 million people are infected by tuberculosis annually, and 1.3 million people died of TB in 2022, according to the World Health Organization (WHO).[2] One of the most prominent reasons for such fatality of this disease is the rise of drug-resistant variants of *Mycobacterium tuberculosis*.[3] The conventional drug delivery system is worsening the problem as it has a low efficiency and poor bioavailability.[4,5] Since the traditional drug delivery system is non-controlled and non-specific, even healthy tissues are affected by the drug dosages, and the targeted infected site receives low concentrations of drug dosage. High-concentration dosage in the form of tablets or capsules fails to fix the problem because it aggravates the side effects by harming healthy cells.[6] To combat the issue, it is necessary to develop novel and effective drug delivery systems with enhanced medicinal profiles and therapeutic agent efficacy. Nanomaterial-based targeted drug delivery systems have gained popularity due to their targeted attack on infected cells while not endangering normal tissues and cells of the body.[7]

Nanotechnology advancements have revolutionized conventional therapies by enhancing the efficacy of drug delivery strategies[8] Nanomaterial-based drug delivery systems have enhanced targeting because their small size, ranging from 1–100 nm, allows them to pass through biological barriers, such as the small intestine and skin, for more effective delivery.[9] On top of that, depending on the drug carrier material, the crystallinity of the drug carrier, and the type of adsorption (chemisorption or physisorption) for different drugs, these nanocarrier/drug complexes release drugs through various mechanisms that ensure a controlled releasing mechanism.

Department of Electrical and Electronic Engineering, Bangladesh University of Engineering and Technology, Dhaka 1205, Bangladesh. E-mail: ahmedzubair@eee.buet.ac.bd

† Electronic supplementary information (ESI) available. See DOI: https://doi.org/10.1039/d3na01095c

‡ These authors contributed equally to calculations.

Multiple studies have shown that pH, temperature, and chemical reaction-controlled release are common mechanisms for explaining the release of pharmaceuticals from nanocarriers.[10,11] From previous studies, different nanomaterial-based targeted drug delivery systems were reported, including silver (Ag) nanoparticles,[12] Janus and dendrimer particles [13] and quantum dots.[14] Different experimental procedures and clinical experiments on animals are ongoing regarding nanomaterial-based drug delivery systems.

The investigation of two-dimensional (2D) nanomaterials in the field of therapies and innovative biomedicine has garnered significant attention in recent times, as they provide efficient techniques for disease diagnosis and drug targeting treatment.[15,16] Graphene and its oxides,[17,18] hexagonal boron nitride[19] and phosphorene[20] were reported to be useful in targeted drug therapy. 2D materials demonstrate an impressive capability in drug delivery with numerous benefits. The use of 2D materials combined with specific pharmaceutical agents exhibited enhanced efficacy in comparison to alternative nanocarriers, such as nanoparticles, nanotubes, and nanowires, because of their lamella structure, which provides a high surface area-to-mass ratio and other unique physicochemical properties.[21–23] The vast surface area ensured highly efficient drug loading.[24] On top of that, 2D nanocarriers have good physical interactions with specific drugs, confirming their proper drug-carrying capability. Transition metal dichalcogenides (TMDs), a group of 2D materials, are very promising in biomedical applications[25,26] along with their high utilization in spintronics[27] and optoelectronics.[28] These materials are widely used in sensing applications as their adsorption performance is superior. Previously, a DFT-based study of the interaction between gas molecules and MoS_2 nanosheets was reported.[29] TMD materials, WSe_2 and MoS_2, were theoretically studied as TiO_2/WSe_2 and TiO_2/MoS_2 nanocomposites for a high-performance gas sensor with excellent adsorption capabilities.[30–32] A machine learning interatomic potential (MLIP) based approach can be beneficial to get the properties of materials.[33] Moreover, TMD materials' superior light and heat conversion efficiencies make them suitable for photo/thermal-induced tumor photothermal and photodynamic therapy.[34]

Many targeted drug delivery systems were studied for cancer disease, whereas their use in TB treatment received recent attention. To combat TB, some antibiotics like isoniazid (INH), pyrazinamide (PZA) and rifampicin (RIF) are used. Since conventional methods fail to treat this disease, targeted drug delivery systems through nanomaterials have attracted huge interest. Nanoparticles like gold (Au)[35] and carbon nanotubes[36] were used to ensure that anti-TB drugs successfully reach infected lung cells and release the drug. However, 2D materials, including TMDs, will increase efficiency as they have larger planar and good loading and releasing capability. TMDs, such as WSe_2 and WS_2, are widely used in electronic and optoelectronic applications.[27,37,38] The monolayers of these materials have direct bandgaps that pave the way for photothermal therapy. WSe_2 and WS_2 are biodegradable and have lower toxicity than graphene and its derivatives.[39,40] These make them good candidates for targeted drug delivery systems. Exploring the suitability of different highly efficient, nontoxic 2D TMD materials in this field is vital. Moreover, TMDs, such as WSe_2 and WS_2, were not explored as drug delivery systems.

This study investigated the interaction between two prominent anti-TB drugs, INH and PZA, with two promising TMD materials, WSe_2 and WS_2, and the possible adsorption of the drugs on these 2D materials. We calculated various orientations of the adsorbed anti-TB drugs to evaluate the thermal stability of drug/2D TMD complexes from the perspective of adsorption energy. Furthermore, we calculated the band structures of pristine materials and the band structures when drugs were adsorbed on their planar surface. This investigation provided insight into their crystal-based interaction. For further comprehension, projected band structures were calculated to determine the orbital contributions of various bands. The density of states of drug atoms on adsorbed complexes was calculated to confirm their interaction with 2D materials. Additionally, we performed Mulliken charge analysis and calculated the electron density difference to know the nature of the bond and interaction of drug atoms and WS_2 and WSe_2. Optical properties were investigated to observe the absorption behavior of drug/2D TMD complexes and to check the suitability of using photothermal therapy. Finally, to investigate the controlled releasing criteria, we calculated the change of adsorption energy with increasing temperature. This study will facilitate designing a nanosystem for targeted and selective anti-TB drug delivery *via* WS_2 and WSe_2 monolayers.

2 Methods

We performed first-principles calculations using density functional theory (DFT),[41] employing generalized gradient approximation (GGA) with the Perdew–Burke–Ernzerhof (PBE) parametrization functional for exchange–correlation interactions and Grimme's DFT-D scheme[42] for van der Waals interactions. At first, we cleaved a monolayer of tungsten diselenide (WSe_2) and tungsten disulfide (WS_2) from bulk hexagonal symmetry (2 H) crystals. Each unit cell consists of three atoms: one tungsten (W) and two selenium (Se) or sulfur (S) atoms. To prevent interlayer interactions, we introduced a 20 Å vacuum. A $(4 \times 4 \times 1)$ supercell, consisting of 48 atoms, was constructed to serve as the nanocarrier for anti-TB drugs such as INH and PZA. The chemical formulae of INH and PZA are $C_5N_3H_5O$ and $C_5N_3H_5O$, respectively. We determined the suitable location and orientation for drug adsorption using the Adsorption Locator module[43] in Materials Studio. We selected the most energetically stable orientation and location of drugs for subsequent relaxation and property calculations. The relaxation process was performed using the CASTEP[44] module in Materials Studio, within a kinetic energy cutoff of 450 eV, Gaussian smearing of 0.04 eV, an ultrasoft pseudopotential for 2D TMDs and drug atoms and a $(3 \times 3 \times 1)$ Γ-centered k-point grid in the Monkhorst–Pack scheme. The iterative procedure was repeated until the convergence threshold of the total energy reached below 10^{-5} eV per atom, the Hellmann–Feynman force among the atoms was below 0.02 eV Å^{-1}, and the stress was below 0.1 GPa. For electronic and optical property calculations, we increased

the sampling in the Monkhorst–Pack k-point grid to $(5 \times 5 \times 1)$ Γ-centered k-points for higher accuracy. We used the DMol3 (ref. 45) module in Materials Studio to determine the adsorption energies (E_{ads}) of the anti-TB drug/WSe$_2$ (WS$_2$) complexes. The adsorption energy was calculated by deducting the energies of the drug molecules and the monolayer WSe$_2$ (WS$_2$) from the energy of the complex, as given by,

$$E_{ads} = E_{drug/2D\ TMD} - E_{2D\ TMD} - E_{drug} \qquad (1)$$

where $E_{2D\ TMD}$, E_{drug}, and $E_{drug/2D\ TMD}$ represent the DFT calculated energies of the pure 2D TMDs, the adsorbed drug molecules, and the adsorbed molecule and 2D TMD drug complexes, respectively. Energetically stable configurations were identified by negative values of E_{ads}, indicating strong exothermic interactions and thermally stable adsorption. The magnitude of E_{ads} quantified the strength of the interaction.

Electronic band dispersion calculations were performed along the $\Gamma\,(0\,0\,0) \rightarrow M\,(0.0\ 0.5\ 0.0) \rightarrow K\,(-0.333\ 0.667\ 0.0) \rightarrow \Gamma$ $(0\ 0\ 0)$ path for energetically stable configurations. The density of states (DOS) calculations were conducted for pure WSe$_2$, pure WS$_2$, drug/monolayer WSe$_2$, and drug/monolayer WSe$_2$. The projection of DOS on various orbitals of all constituent atoms was performed for drug complexes. These calculations were performed through the CASTEP module.

To further understand the nature of adsorption, we performed Mulliken charge analysis [46] and electron density difference (EDD) calculations in CASTEP. Additionally, we calculated the optical properties of the system in CASTEP to analyze the effect of drug adsorption on the 2D sheets. Details of the optical property calculations are provided in the ESI.† Furthermore, we performed orbital projected band structure calculations using the Quantum Espresso simulation package[47,48] to determine the suborbital contributions to the various bands. Moreover, to show the temperature-dependent release of the drugs, we used the Phonopy open source package[49] to determine the temperature-dependent portion of Helmholtz free energy. Through Phonopy, supercells with different displacements of atoms were created. After calculating the self-consistent field (SCF) of each of them, the force set was calculated, and through it, thermodynamic properties, including Helmholtz free energy and temperature-dependent vibrational energy, were estimated. In the Materials Studio, all the calculations were performed at $T = 0$ K. Hence, the adsorption energy was also calculated at $T = 0$ K. We determined temperature-dependent vibrational energy and calculated the adsorption energy for various temperatures.

3   Results

3.1   Geometry structure and adsorption energy for anti-TB drug/2D TMD complexes

We relaxed the pristine structures of WS$_2$, WSe$_2$, INH, and PZA, which are shown in Fig. 1(a)–(d). INH and PZA drugs have a hexagonal plane and tilted –CON$_2$H$_3$ and –CONH$_2$ functional groups. The transition metal tungsten (W) is sandwiched between two chalcogen layers of sulfur (S) atoms in 2 H WS$_2$. The bulk WS$_2$ consists of many layers of monolayer WS$_2$, and

layers are packed due to weak van der Waals forces. A monolayer of WS$_2$ can be found through physical or chemical processes. A hexagonal phase is seen in the WS$_2$ structure where three S atoms are bonded to a single W atom, and prominent coulombic interaction is found between S and W molecules. WSe$_2$ has a similar geometric structure. Lattice constants, the bond length between W and S/Se atoms, and bond angles of two optimized structures were investigated. The results are shown in Table 1. The bond length of W–S was found to be 2.42 Å and for W–Se, the length was 2.53 Å. These results were consistent with previous studies.[28,50] Monolayer WS$_2$ and WSe$_2$ had lattice constants of 3.18 Å and 3.2925 Å, which agreed with previously reported values.[51]

Fig. 1(e)–(i) show the different adsorption configurations of INH and PZA drugs on the monolayer WS$_2$ surface. From top and side views, it is demonstrated that drugs were adsorbed in both horizontal and vertical directions. In Fig. 1(g) it is seen that both drugs were simultaneously adsorbed in the horizontal direction for WS$_2$. Here, the horizontal configuration implies that the drug and 2D TMDs were in a parallel direction, and the vertical configuration means the perpendicular orientation of drug structures. Fig. 1(j)–(n) show the 2D TMD drug complexes of horizontal and vertical adsorption on monolayer WSe$_2$. Table 2 shows the calculated adsorption energy and vertical distances between anti-TB drugs and 2D TMDs. In 2D TMD drug complexes, the configurations suggest that physisorption occurred rather than chemisorption. For vertical structures of drug/2D TMD, we used the notation of drug(V)/2D TMD, and for horizontal structures, we used drug(H)/2D TMD. Drug (V)/WS$_2$ and drug(V)/WSe$_2$ had higher adsorption energies than other configurations, making them metastable. The most thermally stable structure was found when both INH and PZA drugs were adsorbed simultaneously. INH/PZA(H)/WSe$_2$ configuration was the thermally strongest 2D TMD monolayer complex with an adsorption energy of −2.35 eV. PZA(V)/WS$_2$ configuration had the highest adsorption energy of −0.28 eV among the studied configurations. Comparing thermal stability through the formation energy of the structures, INH/PZA(H)/WSe$_2$ > INH/PZA(H)/WS$_2$ > INH(H)/WSe$_2$ > PZA(H)/WS$_2$ > INH(H)/WS$_2$ > PZA(H)/WS$_2$INH(V)/WSe$_2$ > PZA(V)/WS$_2$ > INH(V)/WSe$_2$ > PZA(V)/WS$_2$. If the adsorption energy of a drug/2D TMD complex becomes much lower, then stability may be higher but it will be difficult to release the drug conveniently. So, adsorption energy must be in the moderate range for drug release and structural stability. All the drug(V)/2D TMD complexes had much higher adsorption energy so they might be in a metastable state where their uncontrolled release characteristic is more probable. As a result, we emphasized drug(H)/2D TMD complexes in this paper.

3.2   Electronic properties

3.2.1   WS$_2$ and WSe$_2$ monolayers. We calculated and analyzed the band structures and DOS of horizontally adsorbed drugs on 2D nanocarriers. At first, the band structure and DOS of the monolayer supercells of WS$_2$ and WSe$_2$ were calculated. Fig. 2(a) and (b) show the band structure and DOS of pristine
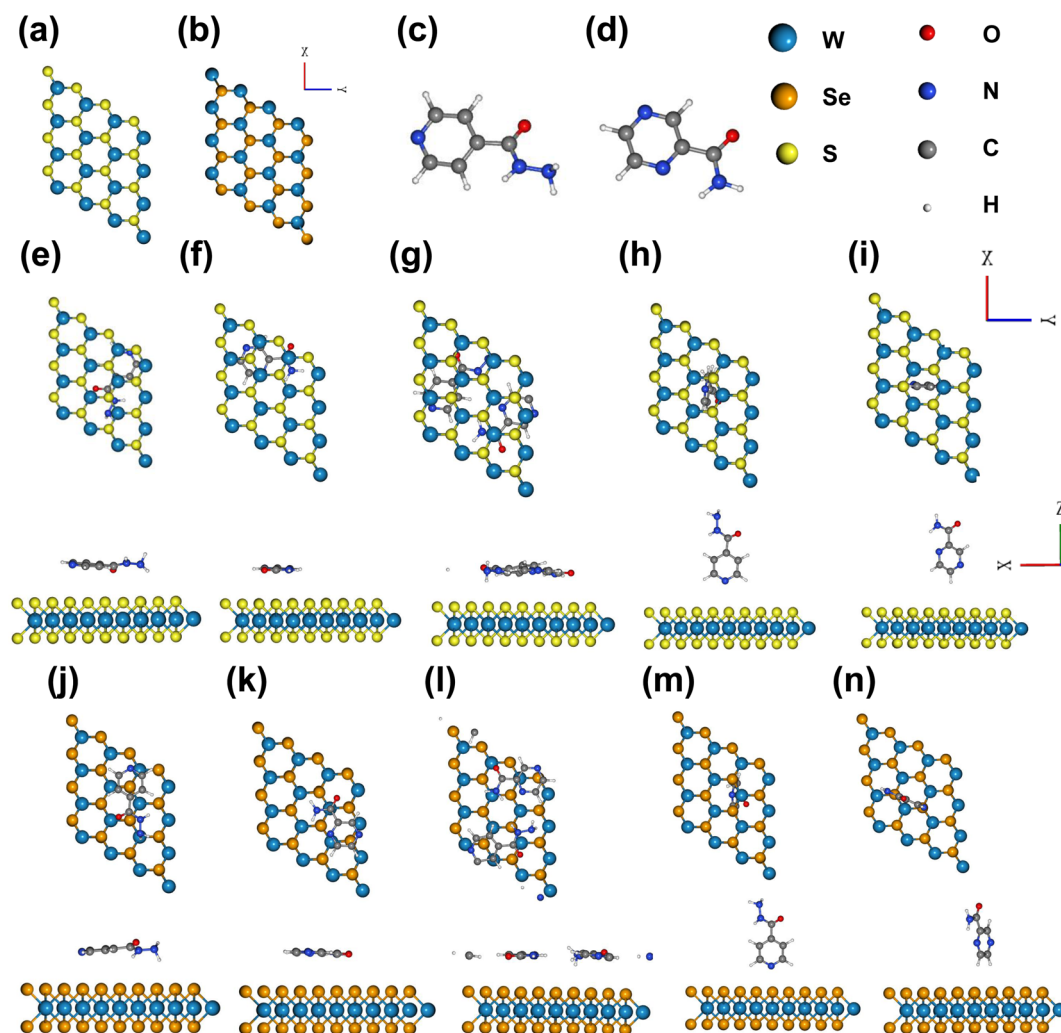
Fig. 1 Optimized structures of (a) WS$_2$, (b) WSe$_2$, (c) INH, and (d) PZA. Top and side views of the optimized TMD complexes of (e) INH(H)/WS$_2$, (f) PZA(H)/WS$_2$, (g) INH/PZA(H)/WS$_2$, (h) INH(V)/WS$_2$, (i) PZA(H)/WS$_2$, (j) INH(H)/WSe$_2$, (k) PZA(H)/WSe$_2$, (l) INH/PZA(H)/WSe$_2$, (m) INH(V)/WSe$_2$, and (n) PZA(V)/WSe$_2$. Here, drug(H) indicates the horizontal position of drug atoms, and drug(V) indicates the vertical position.

Table 1 Calculated structural parameters

Crystal structures	Lattice constant ($a = b$ in Å)	Bond length W–S (Å)	Bond length W–Se (Å)	∠S–W–S	∠Se–W–Se
WS$_2$ ($4 \times 4 \times 1$)	12.72	2.42		80.94°	
WSe$_2$ ($4 \times 4 \times 1$)	13.17		2.53		81.13°

WS$_2$ and WSe$_2$. The bandgap of pristine WS$_2$ was 1.81 eV, and the bandgap of WSe$_2$ was 1.60 eV, and the results matched with previously reported values.[28,52,53] Both of the nanocarriers had a direct bandgap, and the bandgap occurred at the high symmetry K point. However, since the PBE functional underestimates the bandgap, we also calculated the band structures with the HSE06 functional for monolayer TMDs. For WSe$_2$, the calculated bandgap was 2.15, whereas, for the WS$_2$ monolayer, the bandgap was 2.34 eV. These results agreed with previously reported experimental findings.[54] These band structures can be found in the ESI.†

Table 2 Calculated vertical adsorbed distance, d (in Å), adsorption energy, and E_{ads} (in eV unit) of INH and PZA drugs on WS$_2$ and WSe$_2$ surfaces

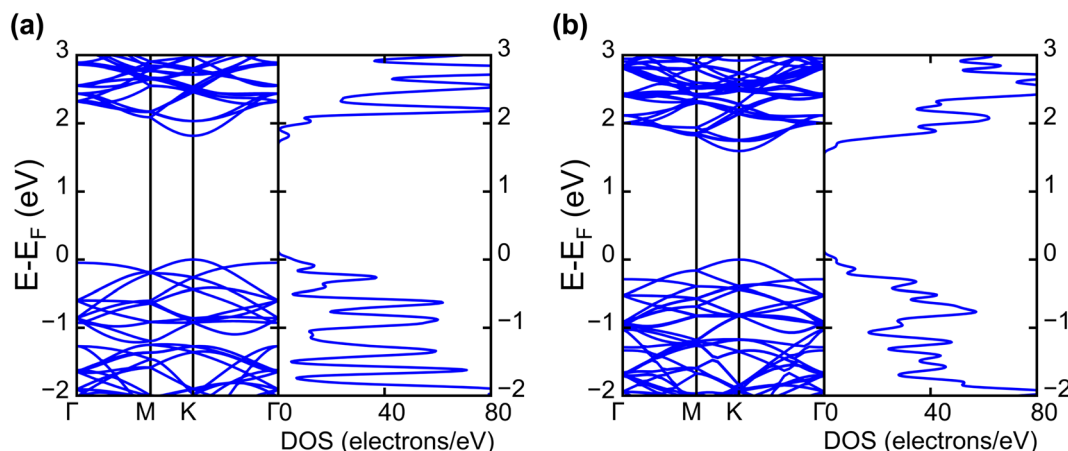|	WS$_2$		WSe$_2$	
	d	E_{ads}	d	E_{ads}
Drug structures	(Å)	(eV)	(Å)	(eV)
INH (H)	3.46	−0.96	3.89	−1.25
PZA (H)	3.38	−0.99	3.59	−1.21
INH/PZA (H)	3.11	−1.97	3.16	−2.35
INH (V)	3.32	−0.48	2.81	−0.80
PZA (V)	3.49	−0.28	2.81	−0.74

Fig. 2 Calculated electronic band structures and corresponding DOS of pristine (a) WS_2 and (b) WSe_2 monolayers.

The band projection on atomic orbitals was performed to understand the band structure better, and the contributions of different orbitals were evaluated. The d-orbitals of the transition metal W atom mainly contributed to the valence and conduction band edges. For WS_2, $d_{x^2-y^2}$ contributed 36.68% and d_{xy} contributed 36.66% to valence band maxima (VBM). Other main contributions to VBM came from the p_x (10.4%) and p_y (10.4%) orbitals of S atoms. The conduction band minima (CBM) mainly consisted of the d_{z^2} orbital, with a contribution of 80.32%. The s orbital of the W atom contributed more than 10% to CBM. For WSe_2, the involvement of d orbitals with their contribution percentage remained almost the same. The $d_{x^2-y^2}$ contributed 38.59% and d_{xy} contributed 38.11% to the valence

band maxima (VBM) of WS_2, while d_{z^2} contributed to 78.69% to CBM. Fig. 3(a) and (b) show the orbital projected band diagram for pristine WS_2 and WSe_2 monolayers.

3.2.2 Drug(H)/2D TMD complexes. For both 2D TMD drug complexes, band structures were dominated by pristine 2D TMD sheets. It was found that the drug atoms did not significantly modify the electronic bands when they were adsorbed on the TMDs. The bandgap of the drug(H)/2D material complexes was almost the same as that of their pristine material. Besides, the direct bandgap behavior of WS_2 and WSe_2 remained the same for all complexes. The DOS of the structures matched with that of the corresponding band structures. Fig. 4(a)–(c) demonstrate WS_2 sheets that adsorbed INH, PZA, and

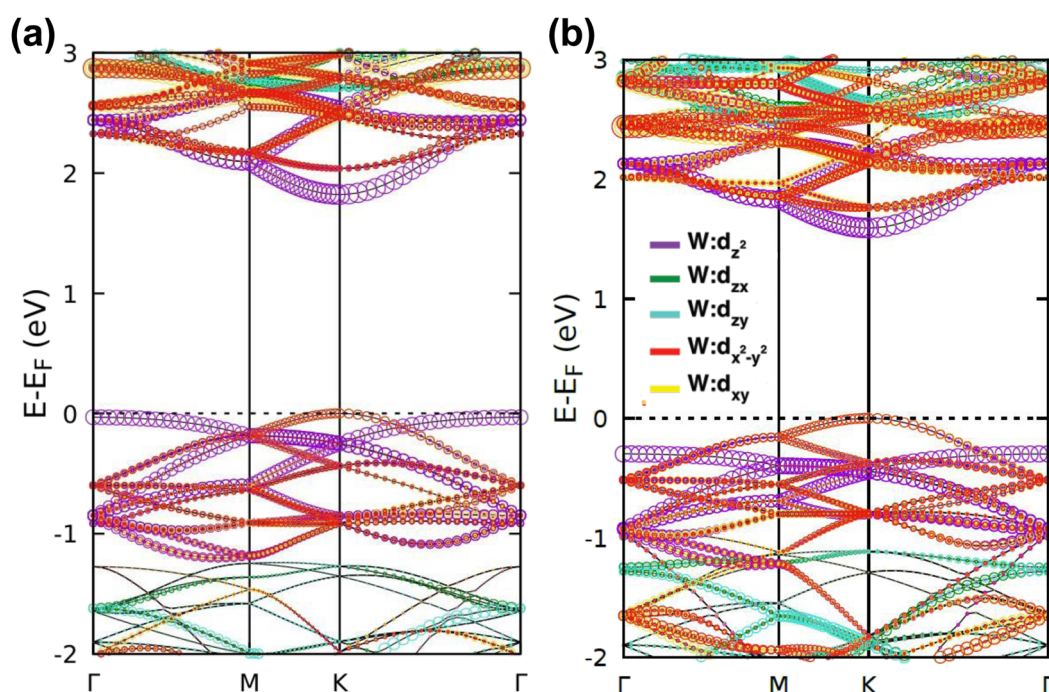Fig. 3 Orbital projected band diagrams showing the contribution of d-orbitals of the W atom of (a) WS_2 and (b) WSe_2. In the figures, the amount of contributions is indicated by the size of the circles, and the corresponding colors illustrate the contributing sub-orbitals.
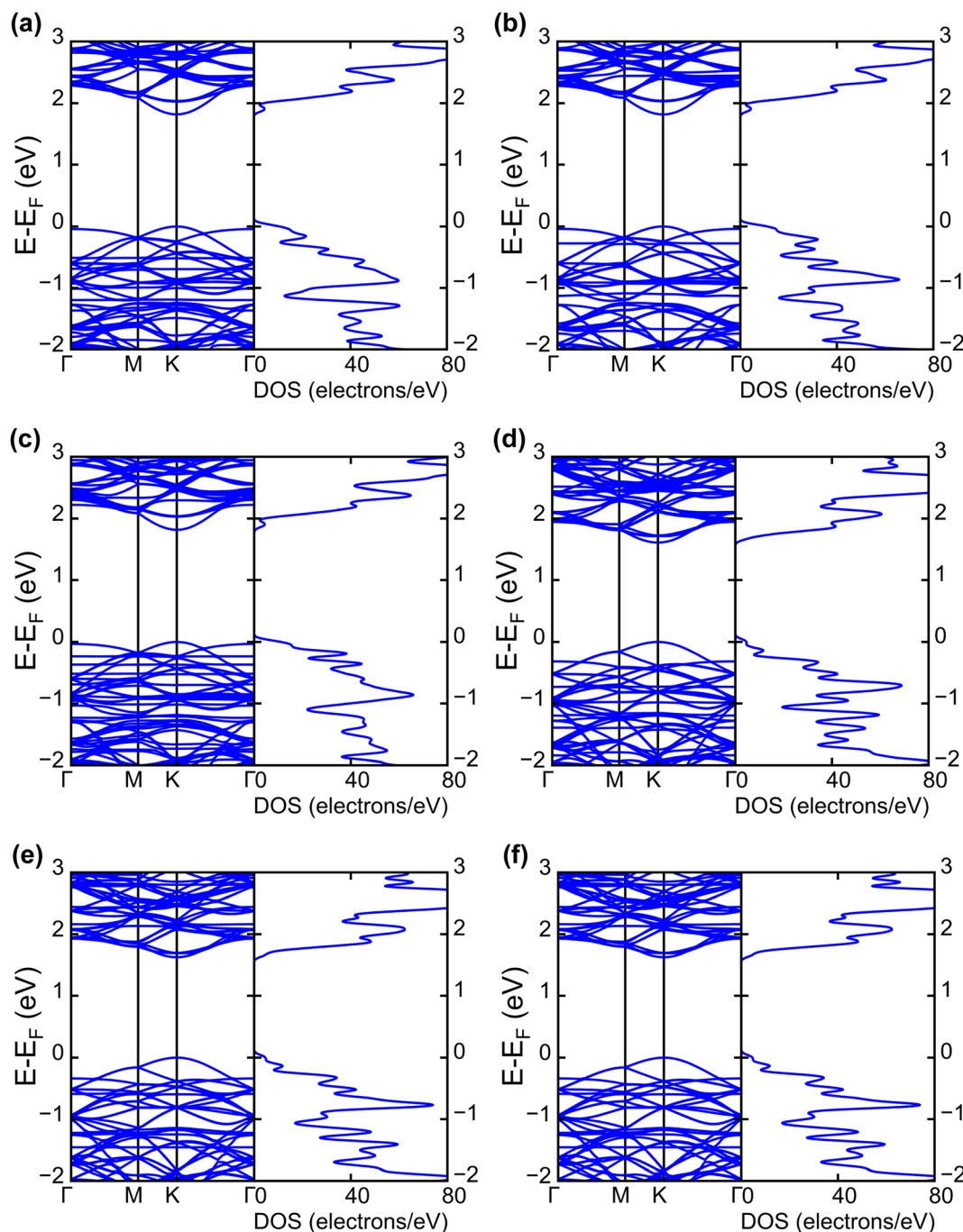
Fig. 4 Electronic band structures and DOS of (a) INH(H)/WS$_2$, (b) PZA(H)/WS$_2$, (c) INH/PZA(H)/WS$_2$, (d) INH(H)/WSe$_2$, (e) PZA(H)/WSe$_2$, and (f) INH/PZA(H)/WSe$_2$.

a combination of INH/PZA, respectively. Fig. 4(d)–(f) show the calculated results for drug absorbed WSe$_2$ complexes. The band structures and DOS of vertically adsorbed INH on WS$_2$ and WSe$_2$ are discussed in the ESI.†

The projected DOS of drug atoms in drug/2D TMD complexes was calculated for further investigation. Fig. 5(a) and (b) depict the DOS of drug atoms in the two structures that were energetically most favorable, INH/PZA(H)/WS$_2$ and INH/PZA(H)/WSe$_2$. As new states of drugs were introduced into the complex

structures, it is evident that interactions occurred between drug atoms and 2D materials. TB drug atoms that were adsorbed did not add new states to the pristine bandgap region, and that's why pristine structures dominated the bandgap of the 2D TMD monolayer complexes. However, drug atoms have added states below the VBM and above the CBM. Besides, it can be seen that the p orbital of the drug atoms predominantly contributed to the new states where the s orbital had little contribution to valence bands and almost negligible presence in conduction
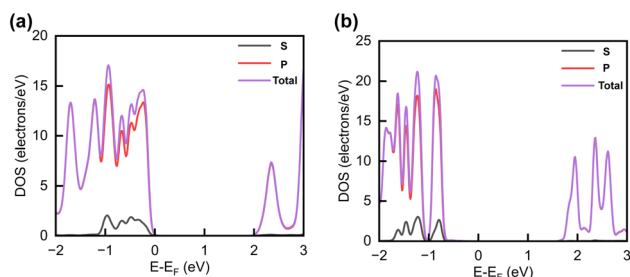
Fig. 5 Calculated projected DOS of INH and PZA drug atoms for (a) INH/PZA(H)/WS₂ and (b) INH/PZA(H)WSe₂.

Table 3 Average Mulliken charge of atoms of WSe₂ drug complexes

Atoms	WSe₂ ($|e|$)	INH(H)/WSe₂ ($|e|$)	PZA(H)/WSe₂ ($|e|$)	INH/PZA(H)/WSe₂ ($|e|$)
H	0.378	0.266	0.292	0.283
C	0	−0.068	0.034	−0.023
N	−0.565	−0.510	−0.520	−0.517
O	−0.575	−0.530	−0.550	−0.535
Se	0.100	0.121	0.113	0.139
W	−0.190	−0.203	−0.196	−0.212

bands. Details of individual drug atoms' contribution to the DOS are discussed in the ESI.† Furthermore, we calculated the projected band structure for those two energetically most stable structures and found that the contributions of d orbitals are almost the same as that of their pristine structures. For INH/PZA(H)/WSe₂, $d_{x^2-y^2}$ contributed 39.65% and d_{xy} contributed 39.65% to VBM where CBM mainly consisted of the d_{z^2} orbital, with a contribution of 80.55%. However, insignificant changes in d suborbital contributions were observed in INH/PZA(H)/WS₂ compared to those of pristine WS₂, as seen in Fig. 6.

3.3 Charge density analysis

After confirming the energy stability of drug adsorption, comprehensive analyses were conducted using Mulliken charge analysis and the electron density difference (EDD) to elucidate the nature and mechanisms of drug adsorption on monolayer WSe₂ and WS₂. Notably, no covalent bonds were formed between the drug molecules and the 2D TMD materials, and the adsorption distances fell within the optimal range of physisorption. We determined the

electron density difference, $\Delta n_{\text{drug/2D TMD}}$, of the 2D TMD complexes before and after the drug molecules' physisorption using the formula below to explore the interaction between molecules and 2D TMDs.

$$\Delta n_{\text{drug/2D TMD}} = n_{\text{drug/2D TMD}} - n_{\text{2D TMD}} - n_{\text{drug}} \quad (2)$$

Mulliken charge transfer analysis revealed that the average charge per atom exhibited slight changes following adsorption. Electrons were transferred from the drug molecules to the drug(H)/2D TMD complex interface, specifically to the electrophilic groups (CON₂H₃ in INH and CONH₂ in PZA) of the drug molecules. The electrophilic groups of INH exhibited an attractive force towards the electrons present in the 2D TMDs. This interaction led to the polarization of the complex situated underneath the adsorption site, thereby inducing intramolecular charge transfer. The transfer of electrons between the drug molecules and the WSe₂ and WS₂ surfaces was not uniform. The atoms in the drug molecules that were closer to the interface experienced the greatest electron transfer, while the atoms that were further away experienced negligible
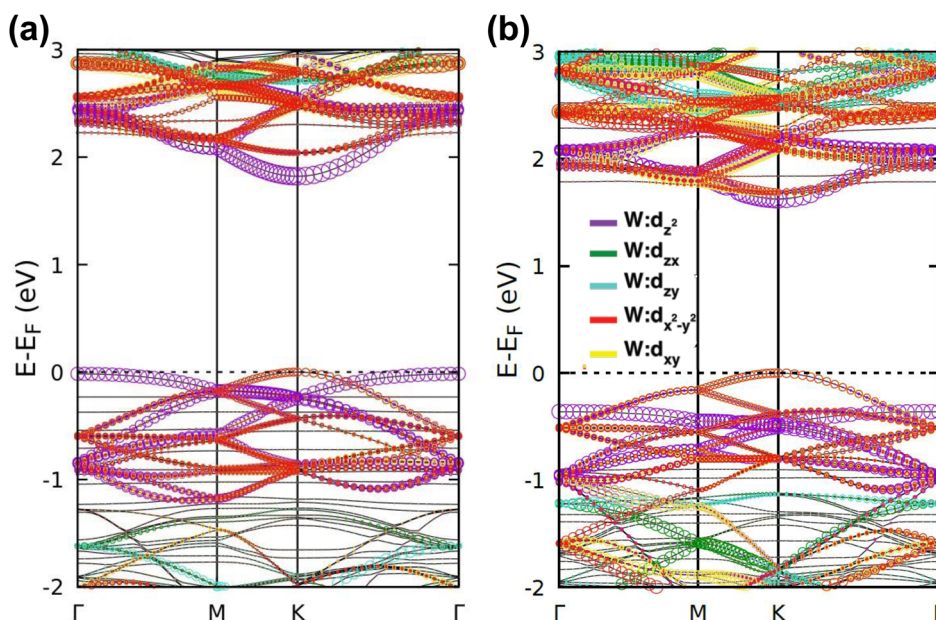

Fig. 6 Orbital projected band diagrams showing the contribution of d orbitals of the W atom for (a) INH/PZA(H)/WS₂ and (b) INH/PZA(H)/WSe₂ are illustrated. In the band diagrams, the amount of contributions is indicated by the size of the circles, and the corresponding colors illustrate the contributing sub-orbitals.

Table 4 Average Mulliken charge of atoms of WS$_2$ drug complexes

Atoms	WS$_2$ ($|e|$)	INH(H)/WS$_2$ ($|e|$)	PZA(H)/WS$_2$ ($|e|$)	INH/PZA(H)/WS$_2$ ($|e|$)
H	0.171	0.356	0.380	0.356
C	0.029	0.061	0.048	−0.003
N	−0.196	−0.540	−0.546	−0.540
O	−0.372	−0.560	−0.590	−0.565
S	−0.030	−0.028	−0.028	−0.024
W	0.060	0.059	0.058	0.059

electron transfer. The average charge density difference for each drug molecule is summarized in Tables 3 and 4.

Drug molecules inside the INH(H)/WSe$_2$ complex demonstrated the most significant gain in electron density, with the C, N, and O atoms gaining 0.068e, 0.055e, and 0.045e, respectively. Conversely, the H atoms in these molecules lost 0.112e. The molecules of the drug within the PZA(H)/WSe$_2$ complex also gained electrons, but the gains were smaller than those observed in the INH(H)/WSe$_2$ complex (0.045e, 0.034e, and 0.025e for N, C, and O atoms, respectively). The H atoms in these molecules also lost electrons, but the losses were also smaller than those observed in the INH(H)/WSe$_2$ complex (0.086e). The drugs contained within the INH/PZA(H)/WSe$_2$ complex showed the greatest gains again, with the N, O, and C atoms gaining 0.048e, 0.040e, and 0.023e, respectively. The H atoms in these molecules also lost electrons, but the losses were similar to those observed in the PZA(H)/WSe$_2$ complex (0.095e).

Drug molecules inside the PZA(H)/WS$_2$ complex gained electrons, with the greatest gains observed for the N and O atoms (0.344e and 0.118e, respectively). Conversely, the H and C atoms in these molecules lost electrons (0.112e and 0.019e). The molecules of the drug within the INH(H)/WS$_2$ complex also gained electrons, but the gains were higher than those observed in the PZA(H)/WS$_2$ complex (0.188e, 0.344e and 0.089e for O, N and C atoms, respectively). The H atoms in these molecules also lost electrons, but the losses were also higher than those observed in the PZA(H)/WS$_2$ complex (0.185e). The drugs contained within the INH/PZA(H)/WS$_2$ complex showed the largest gains in electron density among the three, with the greatest gains again observed for the C, O, and N atoms (0.0315e, 0.193e, and 0.344e respectively). The H atoms in these molecules also lost electrons, but the losses were similar to those observed in the PZA(H)/WS$_2$ complex (0.185e).

Overall, the Mulliken charge transfer analysis results suggest that the drug molecules in all six complexes interacted with the WSe$_2$ and WS$_2$ surfaces similarly, with the greatest electron transfer occurring to the N, C, and O atoms. The H atoms in these molecules lost electrons, but the losses were smaller than those observed for the N, C, and O atoms. This electron sharing was found to be insufficient for the formation of additional covalent bonds but adequate for physisorption. Fig. 7 visually depicts the accumulation of electrons on the Se and S atoms, while the drug functional groups experienced a depletion of electrons. Here, an iso-surface value of 0.1 was used. Considering the significant adsorption distances and the low magnitude of charge transfer, it
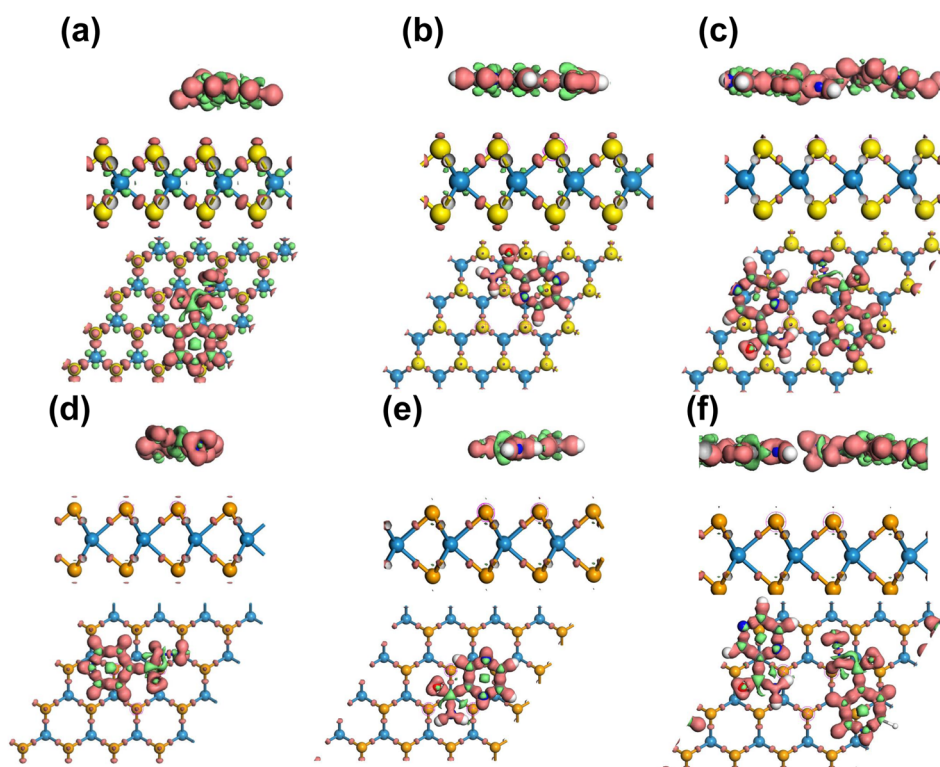

Fig. 7 Electron density difference plots of (a) INH(H)/WS$_2$, (b) PZA(H)/WS$_2$, (c) INH/PZA(H)/WS$_2$, (d) INH(H)/WSe$_2$, (e) PZA(H)/WSe$_2$, and (f) INH/PZA(H)/WSe$_2$. Red and green colors depict the accumulation and depletion of electron density of the structures. The iso-surface value is 0.1.

can be concluded that the drug molecules undergo physisorption on the WSe$_2$ and WS$_2$ monolayers.

3.4 Optical properties

The WSe$_2$ and WS$_2$ drug complexes can be used in phototherapy. In this regard, the optical properties of WSe$_2$ and WS$_2$ and their drug complexes were calculated. The absorption

coefficient *vs.* wavelength is a critical parameter for nanomaterial-based drug delivery systems. Absorption coefficients are calculated from the imaginary part of the complex dielectric constant of pristine structures and their complexes. (See the ESI for the detailed formulation†). The relationship between the absorption coefficient, α, and dielectric constants, ε_1 and ε_2, is given by the following equation.
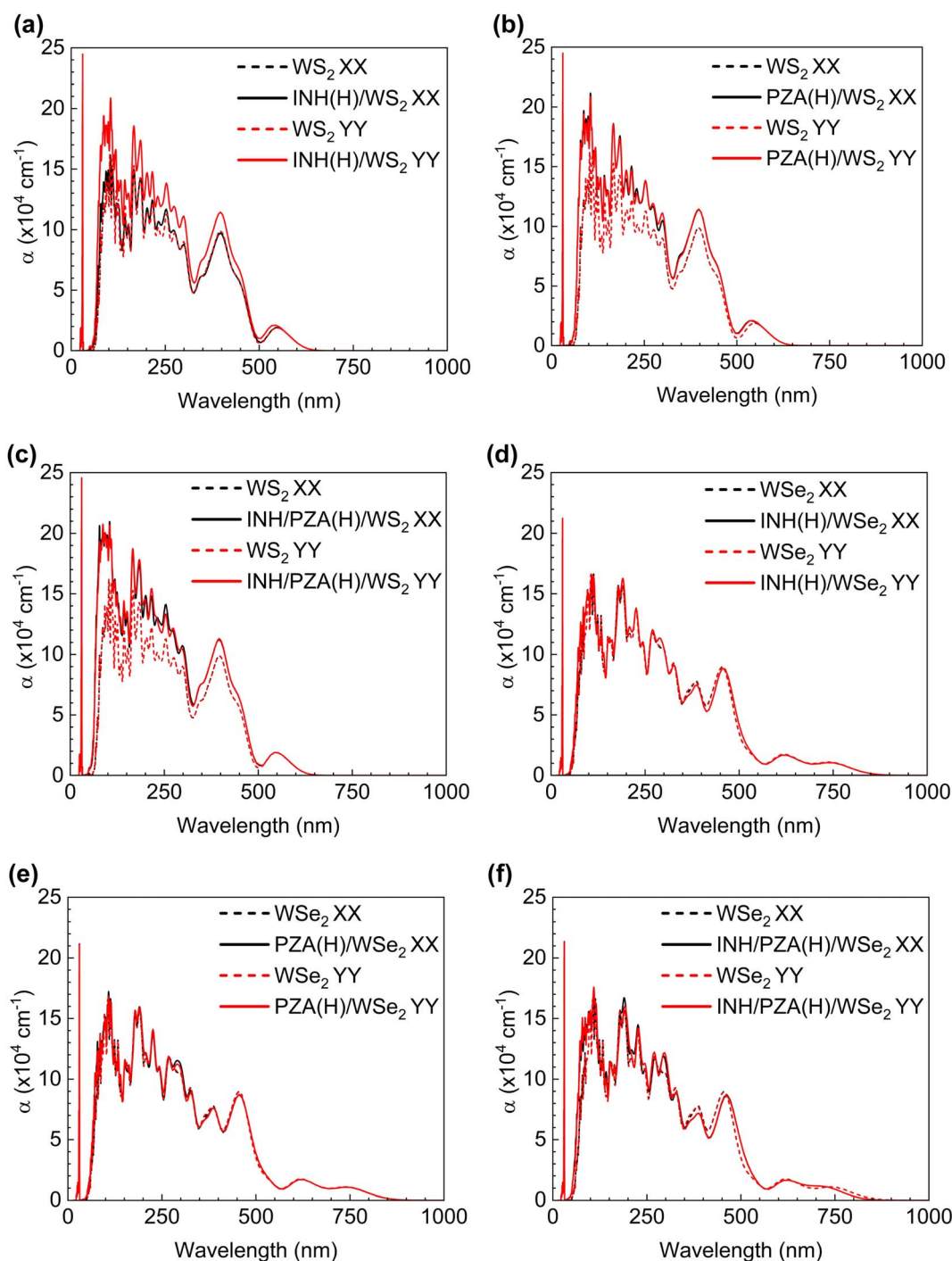

Fig. 8 Absorption coefficient, α *vs.* wavelength figure for (a) INH(H)/WS$_2$, (b) PZA(H)/WS$_2$, (c) INH/PZA(H)/WS$_2$, (d) INH(H)/WSe$_2$, (e) PZA(H)/WSe$_2$, and (f) INH/PZA(H)/WSe$_2$; in every figure the corresponding pristine WS$_2$ or WSe$_2$ trend is denoted by a dotted line to visualize the comparison between graphs.

$$\alpha(\omega) = \frac{4\pi\kappa(\omega)}{\lambda} = \frac{4\pi}{\lambda\sqrt{2}}\left(\sqrt{\varepsilon_1^2(\omega) + \varepsilon_2^2(\omega)} - \varepsilon_1(\omega)\right)^{1/2}, \quad (3)$$

here, κ is the extinction coefficient and λ is the wavelength.

For the drug complexes to be utilized in photothermal therapy, there should be good absorption within the visible range (wavelengths of 400–700 nm) or near-infrared (NIR) range (700–1350 nm).[55] This is because we cannot use light of all wavelengths on the body as it will damage the tissues and cells. Fig. 8(a)–(f) show the optical behavior of drug(H)/WS$_2$ and drug(H)/WSe$_2$ complexes compared with the pristine behavior. It is evident that a good absorption peak was found in both the visible range and the NIR range for drug (H)/WSe$_2$ structures. However, for drug(H)/WS$_2$ structures, a notable peak is found only within the visible light range. The PZA and INH structures have a noteworthy absorption peak between 3.5 and 4.0 eV.[20] When they were adsorbed by WSe$_2$ or WS$_2$, the 2D TMD dominated their characteristics, and this aligned with the absorption coefficient figures too. When polarized light in the x or y direction passed through the pristine and drug(H)/2D TMD complexes, the absorption behavior was investigated. The pristine WSe$_2$ structure had the same absorption behavior in both directions, and absorption started from the onset of the bandgap. WSe$_2$ drug complexes also showed the same trend. For pristine WS$_2$ absorption started from the edge of the corresponding bandgap wavelength, regardless of whether y or x polarized light was incident on it. Drug(H)/WSe$_2$ complexes showed a similar tendency.

The utilization of NIR photothermal therapy is not feasible for drug(H)/WS$_2$ structures because of the absence of a strong absorption peak within the NIR spectral range (700–1350 nm). Finally, it can be said that photothermal therapy can be achievable with both drug(H)/WS$_2$ and drug(H)/WSe$_2$ structures, regardless of whether x or y polarized light was incident. However, photothermal therapy with the NIR range can be achievable only for drug(H)/WSe$_2$ structures. In this regard, WSe$_2$ drug complexes are in a better place since the use of NIR is highly appreciable in photothermal therapy due to better biological penetration of NIR light in the body.[56]

3.5 Release of drug molecules

After optical radiation is applied in photothermal therapy, releasing drug compounds from drug/2D TMD structures is critical in targeted drug delivery systems. Hence, adsorption energy should be a function of temperature in this case. The previous calculations of adsorption energy were done at $T = 0$ K with the idealized criteria and omitting the thermal vibrational component of the system. In temperature-controlled studies, such as drug delivery in photothermal treatment, it is imperative to consider the Helmholtz free energy (F) as the essential thermodynamic potential. Consequently, the thermal corrections in the adsorption energy were determined by considering the phonon vibration modes as quantum harmonic oscillators. Vibrational energy is temperature-dependent, and adding it to ideal adsorption energy will give a more accurate result. Vibrational energy was calculated with the "finite difference method".
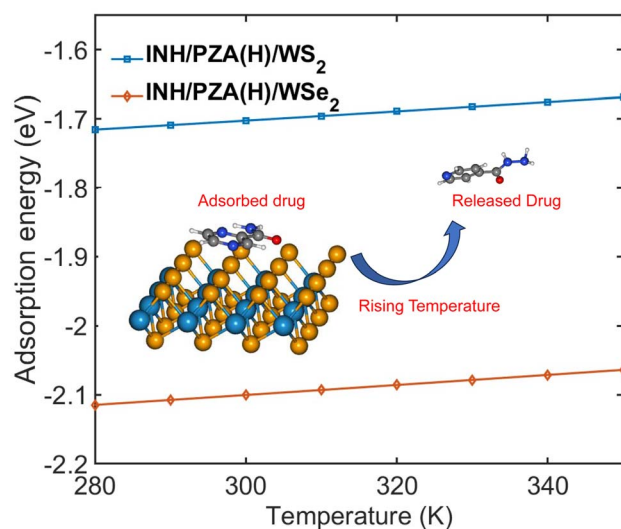

Fig. 9 Temperature dependent adsorption energy of INH/PZA(H)/WS$_2$ and INH/PZA(H)/WSe$_2$ complexes.

$$F = E_{\text{DFT}} + A_{\text{vibrational}} \quad (4)$$

Fig. 9 demonstrates the change of adsorption energy with temperature. Both drug/2D TMD complexes showed an increase in adsorption energy with the increase in temperature. The INH/PZA(H)/WS$_2$ graph shows a 0.3034 eV increase in adsorption energy when temperature increased from 0 to 350 K, where the INH/PZA(H)/WSe$_2$ complex demonstrated a 0.2861 eV increase in energy. The rise of adsorption energy will enable a temperature-controlled release of anti-TB drug molecules. Since the formation energy (or adsorption energy of drug molecules) of 2D TMD complexes was rising, the probability of the anti-TB drug compound being isolated from weakly physisorbed interaction is higher. This method of temperature-dependent adsorption energy calculation was reported previously.[20] Moreover, this temperature-controlled releasing mechanism is experimentally proven for other 2D material-based targeted drug delivery systems. For example, a multifunctional MoS$_2$-based targeted drug delivery system for tumor cells was successfully synthesized, and the drug was released with photothermal therapy in the NIR region.[57]

4 Conclusion

We systematically investigated the interaction between two anti-TB drugs and two nanocarriers, WS$_2$ and WSe$_2$ monolayers, using DFT calculations. Our results suggested that all the drug/2D TMD complexes were stable because of their favorable adsorption energy. The most stable structure was found when INH and PZA drugs were simultaneously adsorbed on a TMD sheet. Further analysis of bands and DOSs suggested that band structures were mainly dominated by pristine TMD materials, which were more comprehensively understood by projected band structures. Moreover, EDD and Mulliken charge analysis of the drug(H)/TMD complexes ensured that no chemical bond was formed between drug atoms and 2D TMD materials. This

suggests that both drugs can be easily released to the targeted site. Optical analysis showed that drug(H)/WS$_2$ complexes had good absorption within the visible range and drug(H)/WSe$_2$ had good absorption peaks within the NIR range. This shows the possibility of using photothermal therapy with our drug delivery system. Finally, we showed the temperature-dependent releasing mechanism of our TMD material complexes and ensured that the discussed anti-TB drugs could be released by creating heat through photothermal therapy. Our proposed targeted drug delivery system consisting of WS$_2$ or WSe$_2$ sheets showed great promise regarding their potential applications in photothermal therapy and temperature-dependent releasing behavior. The integration of combined photothermal therapy and chemotherapy treatments could revolutionize the field of TB therapy, paving the way for more effective and tailored approaches to combat this deadly disease.

Author contributions

Khaled Mahmud: conceptualization, formal analysis, methodology, visualization, software, investigation, and writing – original draft. Taki Yashir: methodology, visualization, software, and investigation. Ahmed Zubair: supervision, conceptualization, methodology, visualization, project administration, resources, writing – original draft, and writing – review & editing.

Conflicts of interest

There are no conflicts to declare.

Acknowledgements

Notes and references

1 G. Delogu, M. Sali and G. Fadda, *Mediterr. J. Hematol. Infect. Dis.*, 2013, **5**, e2013070.

2 https://www.who.int/news-room/fact-sheets/detail/tuberculosis.

3 P. E. Almeida Da Silva and J. C. Palomino, *J. Antimicrob. Chemother.*, 2011, **66**, 1417–1430.

4 T. L. Andresen, S. S. Jensen and K. Jørgensen, *Prog. Lipid Res.*, 2005, **44**, 68–97.

5 F. Laffleur and V. Keckeis, *Int. J. Pharm.*, 2020, **590**, 119912.

6 T. Schaberg, K. Rebhan and H. Lode, *Eur. Respir. J.*, 1996, **9**, 2026–2030.

7 J. Jacob, J. T. Haponiuk, S. Thomas and S. Gopi, *Mater. Today Chem.*, 2018, **9**, 43–55.

8 R. Dhankhar, S. P. Vyas, A. K. Jain, S. Arora, G. Rath and A. K. Goyal, *Artif. Cells, Blood Substitutes, Biotechnol.*, 2010, **38**, 230–249.

9 H. Cheng, A. Chawla, Y. Yang, Y. Li, J. Zhang, H. L. Jang and A. Khademhosseini, *Drug discovery today*, 2017, **22**, 1336–1350.

10 C. Alvarez-Lorenzo and A. Concheiro, *Chem. Commun.*, 2014, **50**, 7743–7765.

11 L.-T. Fan and S. K. Singh, *Controlled Release: A Quantitative Treatment*, Springer Science & Business Media, 2012, vol. 13.

12 P. Prasher, M. Sharma, H. Mudila, G. Gupta, A. K. Sharma, D. Kumar, H. A. Bakshi, P. Negi, D. N. Kapoor, D. K. Chellappan, *et al.*, *Colloid Interface Sci. Commun.*, 2020, **35**, 100244.

13 V. Percec, D. A. Wilson, P. Leowanawat, C. J. Wilson, A. D. Hughes, M. S. Kaucher, D. A. Hammer, D. H. Levine, A. J. Kim, F. S. Bates, *et al.*, *Science*, 2010, **328**, 1009–1014.

14 C. T. Matea, T. Mocan, F. Tabaran, T. Pop, O. Mosteanu, C. Puia, C. Iancu and L. Mocan, *Int. J. Nanomed.*, 2017, 5421–5431.

15 M. Qiu, W. X. Ren, T. Jeong, M. Won, G. Y. Park, D. K. Sang, L.-P. Liu, H. Zhang and J. S. Kim, *Chem. Soc. Rev.*, 2018, **47**, 5588–5601.

16 D.-K. Ji, C. Ménard-Moyon and A. Bianco, *Adv. Drug Delivery Rev.*, 2019, **138**, 211–232.

17 J. Liu, L. Cui and D. Losic, *Acta Biomater.*, 2013, **9**, 9243–9257.

18 S. Song, H. Shen, Y. Wang, X. Chu, J. Xie, N. Zhou and J. Shen, *Colloids Surf., B*, 2020, **185**, 110596.

19 I. V. Sukhorukova, I. Y. Zhitnyak, A. M. Kovalskii, A. T. Matveev, O. I. Lebedev, X. Li, N. A. Gloushankova, D. Golberg and D. V. Shtansky, *ACS Appl. Mater. Interfaces*, 2015, **7**, 17217–17225.

20 W. Liang and X. Luo, *J. Phys. Chem. C*, 2020, **124**, 8279–8287.

21 J. Shi, P. W. Kantoff, R. Wooster and O. C. Farokhzad, *Nat. Rev. Cancer*, 2017, **17**, 20–37.

22 L. Peng, X. Mei, J. He, J. Xu, W. Zhang, R. Liang, M. Wei, D. G. Evans and X. Duan, *Adv. Mater.*, 2018, **30**, 1707389.

23 Y. Wang, M. Qiu, M. Won, E. Jung, T. Fan, N. Xie, S.-G. Chi, H. Zhang and J. S. Kim, *Coord. Chem. Rev.*, 2019, **400**, 213041.

24 H. Zhang, T. Fan, W. Chen, Y. Li and B. Wang, *Bioact. Mater.*, 2020, **5**, 1071–1086.

25 S. Anju and P. Mohanan, *Synth. Met.*, 2021, **271**, 116610.

26 S. Zhu, L. Gong, J. Xie, Z. Gu and Y. Zhao, *Small Methods*, 2017, **1**, 1700220.

27 K. S. Hoque and A. Zubair, *ACS Omega*, 2022, **7**, 36184–36194.

28 I. M. Ifti, M. M. Hasan, M. A. H. Arif and A. Zubair, *2020 11th International Conference on Electrical and Computer Engineering (ICECE)*, 2020, pp. 391–394.

29 A. Abbasi, A. Abdelrasoul and J. J. Sardroodi, *Adsorption*, 2019, **25**, 1001–1017.

30 A. Abbasi and J. J. Sardroodi, *Comput. Theor. Chem.*, 2017, **1114**, 8–19.

31 A. Abbasi and J. J. Sardroodi, *J. Nanostruct. Chem.*, 2016, **6**, 309–327.

32 A. Abbasi and J. J. Sardroodi, *Appl. Surf. Sci.*, 2019, **469**, 781–791.

33 B. Mortazavi, M. Silani, E. V. Podryabinkin, T. Rabczuk, X. Zhuang and A. V. Shapeev, *Adv. Mater.*, 2021, **33**, 2102807.

34 H. Chen, T. Liu, Z. Su, L. Shang and G. Wei, *Nanoscale Horiz.*, 2018, **3**, 74–89.

35 H. R. Ali, M. R. Ali, Y. Wu, S. A. Selim, H. F. Abdelaal, E. A. Nasr and M. A. El-Sayed, *Bioconjugate Chem.*, 2016, **27**, 2486–2492.

36 N. K. Jain, V. Mishra and N. K. Mehra, *Expert Opin. Drug Delivery*, 2013, **10**, 353–367.

37 S. G. Utsha, S. M. T.-S. Afrid and A. Zubair, *2022 12th International Conference on Electrical and Computer Engineering (ICECE)*, 2022, pp. 168–171.

38 S. M. Ta-Seen Afrid, S. Goswami Utsha and A. Zubair, *2022 IEEE International Conference of Electron Devices Society Kolkata Chapter (EDKCON)*, 2022, pp. 319–324.

39 J. H. Appel, D. O. Li, J. D. Podlevsky, A. Debnath, A. A. Green, Q. H. Wang and J. Chae, *ACS Biomater. Sci. Eng.*, 2016, **2**, 361–367.

40 W. Z. Teo, E. L. K. Chng, Z. Sofer and M. Pumera, *Chem. –A Euro. J.*, 2014, **20**, 9627–9632.

41 E. Engel, *Density Functional Theory*, Springer, 2011.

42 S. Grimme, J. Antony, S. Ehrlich and H. Krieg, *J. Chem. Phys.*, 2010, **132**, 154104.

43 R. L. Akkermans, N. A. Spenley and S. H. Robertson, *Mol. Simul.*, 2013, **39**, 1153–1164.

44 S. J. Clark, M. D. Segall, C. J. Pickard, P. J. Hasnip, M. I. Probert, K. Refson and M. C. Payne, *Z. Kristallogr. Cryst. Mater.*, 2005, **220**, 567–570.

45 B. Delley, *J. Chem. Phys.*, 2000, **113**, 7756–7764.

46 R. S. Mulliken, *J. Chem. Phys.*, 1955, **23**, 1833–1840.

47 P. Giannozzi, S. Baroni, N. Bonini, M. Calandra, R. Car, C. Cavazzoni, D. Ceresoli, G. L. Chiarotti, M. Cococcioni, I. Dabo, *et al.*, *J. Phys.: Condens.Matter*, 2009, **21**, 395502.

48 P. Giannozzi, O. Andreussi, T. Brumme, O. Bunau, M. B. Nardelli, M. Calandra, R. Car, C. Cavazzoni, D. Ceresoli, M. Cococcioni, *et al.*, *J. Phys.: Condens.Matter*, 2017, **29**, 465901.

49 A. Togo and I. Tanaka, *Scr. Mater.*, 2015, **108**, 1–5.

50 B. Amin, T. P. Kaloni and U. Schwingenschlögl, *RSC Adv.*, 2014, **4**, 34561–34565.

51 W. S. Yun, S. Han, S. C. Hong, I. G. Kim and J. Lee, *Phys. Rev. B*, 2012, **85**, 033305.

52 R. Chaurasiya, A. Dixit and R. Pandey, *Superlattices Microstruct.*, 2018, **122**, 268–279.

53 C. Ernandes, L. Khalil, H. Almabrouk, D. Pierucci, B. Zheng, J. Avila, P. Dudin, J. Chaste, F. Oehler, M. Pala, *et al.*, *npj 2D Mater. Appl.*, 2021, **5**, 7.

54 M. Yankowitz, D. McKenzie and B. J. LeRoy, *Phys. Rev. Lett.*, 2015, **115**, 136803.

55 X. Li, J. F. Lovell, J. Yoon and X. Chen, *Nat. Rev. Clin. Oncol.*, 2020, **17**, 657–674.

56 Y. Zhang, S. Zhang, Z. Zhang, L. Ji, J. Zhang, Q. Wang, T. Guo, S. Ni, R. Cai, X. Mu, *et al.*, *Front. Chem.*, 2021, **9**, 728066.

57 C. Zhang, D. Zhang, J. Liu, J. Wang, Y. Lu, J. Zheng, B. Li and L. Jia, *J. Nanobiotechnol.*, 2019, **17**, 1–15.